The regulatory landscape of *Arabidopsis thaliana* roots at single-cell resolution

Authors: Michael W. Dorrity[1], Cristina M. Alexandre[1], Morgan Hamm[1], Anna-Lena Vigil[3], Stanley Fields[1,2], Christine Queitsch[1] and Josh Cuperus[1]

Affiliations:
[1] Department of Genome Sciences, University of Washington, Seattle, WA 98195
[2] Department of Medicine, University of Washington, Seattle, WA 98195
[3] School of Life Sciences, University of Nevada, Las Vegas, NV 89154

[†] Correspondence to Christine Queitsch (queitsch@uw.edu) and Josh Cuperus (cuperusj@uw.edu)

Abstract: In plants, chromatin accessibility – the primary mark of regulatory DNA – is relatively static across tissues and conditions. This scarcity of accessible sites that are dynamic or tissue-specific may be due in part to tissue heterogeneity in previous bulk studies. To assess the effects of tissue heterogeneity, we apply single-cell ATAC-seq to *A. thaliana* roots and identify thousands of differentially accessible sites, sufficient to resolve all major cell types of the root. However, even this vast increase relative to bulk studies in the number of dynamic sites does not resolve the poor correlation at individual loci between accessibility and expression. Instead, we find that the entirety of a cell's regulatory landscape and its transcriptome each capture cell type identity independently. We leverage this shared information on cell identity to integrate accessibility and transcriptome data in order to characterize developmental progression, endoreduplication and cell division in the root. We further use the combined data to characterize cell type-specific motif enrichments of large transcription factor families and to link the expression of individual family members to changing accessibility at specific loci, taking the first steps toward resolving the direct and indirect effects that shape gene expression. Our approach provides an analytical framework to infer the gene regulatory networks that execute plant development.

Introduction

Single-cell genomics allows an unbiased sampling of cells during development, with the potential to reveal the order and timing of gene regulatory and gene expression events that specify cell identity and lineage. An ideal system to test the ability of single-cell genomics to provide novel insights into development is the *Arabidopsis thaliana* root: along its longitudinal axis, a single, radially-symmetric root captures developmental trajectories for several radially-symmetric cell types. Approaches in this organism have included single-cell RNA-seq to transcriptionally profile individual root cell types along this developmental axis[1–6] and with respect to their ploidy.

Studies of chromatin accessibility in samples enriched for specific plant cell types have revealed: (i) the existence of cell type-specific regulatory elements; (ii) the relative scarcity of such elements compared to their prevalence in animals or humans; (iii) the expected enrichment of transcription factor binding sites within these elements; and (iv) a higher frequency of dynamic regulatory elements upstream of environmentally-responsive genes than constitutively expressed genes.[7,8] Although the correlation between chromatin accessibility and nearby gene expression is generally weak in both plants and animals,[9] this correlation improves for regulatory elements that show dynamic changes in chromatin accessibility, for example in response to an environmental stimulus or developmental signal.[7,9–11] In contrast to animals, however, the majority of chromatin-accessible sites in plants show little change across tissues, conditions, or even genetic backgrounds, raising the possibility that cell and tissue identity is less rigidly engrained in the chromatin landscape in plants than in animals.[7] Alternatively, cell type-specific regulatory elements and gene expression in plants may have been obscured by tissue heterogeneity in bulk tissue studies.

Cell type-specific chromatin-accessible landscapes are also of interest for addressing other fundamental biological questions. General transcription decreases along a cell type's developmental trajectory while expression of cell type-specific genes increases,[2,12,13] in agreement with Waddington's predictions on epigenetic landscapes.[14] In the *A. thaliana* root, the increasing maturity of certain cell layers is accompanied by endoreduplication. The presence of additional gene copies may contribute to the observed increase in the expression of cell type-specific genes; alternatively, the initial gene copies may increase their transcription. Although endoreduplication is a common mechanism to regulate cell size and differentiation in plants and some human and animal tissues,[15–17] the influence of this phenomenon on gene regulation and expression has been largely overlooked. In plants, endoreduplication generally enhances transcription,[17,18] in particular of cell wall-related genes[19] and genes encoding ribosomal RNA,[20] hinting at a role for this process in driving increased translation.

Here, we provide the first single-cell resolution maps of open chromatin in the *A. thaliana* root to address the issue of tissue heterogeneity and to detect likely endoreduplication events. We use a droplet-based approach to profile over 5000 nuclei for chromatin accessibility and identify 8000 regulatory elements that together define most cell types of the root. We describe an analytical framework that links patterns of open chromatin with transcriptional states to predict the identity, function and developmental stage of individual cells in the *A. thaliana* root. We integrate the single-cell ATAC-seq (scATAC-seq) data with published single-cell RNA-seq (scRNA-seq) profiles of the same tissue to obtain automated annotations of cells in our scATAC-seq data. Using the integrated dataset, we link individual cells from our scATAC-seq data with their nearest neighbors in scRNA space to define relative developmental progression, level of endoreduplication and the genes differentially expressed in these nearest neighbors. This approach allows the identification of three distinct

developmental states of endodermis cells that had escaped detection using scRNA-seq alone. Using scATAC-seq data integrated scRNA-seq data, we predict individual members of large transcription factor families that play a role in epidermis development, pinpointing individual regulatory events that link peak accessibility and transcription factor expression in these cells. The combination of binding motifs, transcription factor expression and chromatin accessibility provides a basis for predicting the gene regulatory events that underlie development.

Results

scATAC-seq identifies known root cell types

We first asked if ATAC-seq profiles at the single-cell level were capable of capturing known root cell types. We profiled 5283 root nuclei, at a median of 7290 unique ATAC inserts per nucleus. A high fraction of these inserts occurred in one of the 22,749 open chromatin peaks (FRIP score = 0.71) based on pseudo-bulk peak calling (Cellranger v3.1, 10X Genomics); this fraction is similar to that seen in high-quality bulk accessibility studies (**Figure S1A, S1B**).[9] Furthermore, the scATAC assay detected 1794 peaks that not been observed at appreciable levels in bulk ATAC-seq. We used UMAP dimensionality reduction of the peak by cell matrix to build a two-dimensional representation grouping of cells with similar accessibility profiles (**Figure 1A**). Subsequent cluster assignment by Louvain community detection identified nine distinct cell clusters.[21] Across all cells, we identified 4389 peaks (ranging from 307 – 1993 per cell type) with significant differential accessibility, suggesting that around 20% of all accessible sites contain some information on cell type (**Supplementary Table 1**). Though only 16% (707/4,389) of cell type-specific peaks were found to be distal, or greater than 400 base pair from the nearest gene, this was greater than the fraction expected by chance. Only 9.4% (2,159/22,749) of all peaks were distal, suggesting that these distal peaks are slightly (1.7x) enriched for regulatory sites that define cell identity. To assign cell type annotations to each of these clusters, we generated “gene activity” scores that sum all ATAC inserts within each gene body and 400 bp upstream of its transcription start site. This approach rests on the assumption that a chromatin-accessible site in the compact *A. thaliana* genome tends to be associated with regulation of its most proximal gene.[22] While this assumption may not hold universally, gene activity scores offer the advantage of allowing a direct comparison to bulk ATAC-seq and single-cell RNA-seq datasets through a matched feature set. In this way, we identified genes whose accessibility signal specifically marks each cell cluster. We visualized peaks with cell type-specific accessibility by grouping cells of a similar type and “pseudo-bulking” their insert counts at each position in the genome (**Figure 1B**). Bulk and cell type-specific ATAC signal is similar to those obtained in prior whole tissue and cell type enrichment-based ATAC-seq studies for the root (**Figure S1B, S1C, S1D**).[11]

We used comparisons to tissue-specific genes that were identified from single-cell RNA-seq studies of the *A. thaliana* root to assign a cell type to each cluster defined by ATAC markers from "gene activity" scores.[2,5,6] We identified 210 genes with unique accessibility patterns across all cell types (**Supplementary Table 2**); FRIP scores, fragment lengths, and total read counts did not vary greatly across cell types (**Figure S1E, S1F, S1G**). For each cell type, the median number of genes with tissue-specific accessibility was 20 (range 5 to 53) (**Figure 1C**). This small number of genes is consistent with earlier studies that show few open chromatin sites that define cell type identity in *A. thaliana*.[7,23] Although thousands of differentially accessible sites have been found across tissue types,[7] accessibility differences between more closely related cell types remains largely unexplored, with the exception of root hair vs non-hair, in which few differences were found.[7,11] These differences, uncovered using a cell-enrichment based technology,[11] were replicated in the epidermal cells identified in our scATAC assay (**Figure S1C, S1D**). For three cell clusters (959 cells, or 18% of cells), we could not identify a coherent set of a markers and therefore could not annotate them (grey points, **Figure 1A**). However, all other cell clusters were manually annotated and corresponded to the major cell layers of the root (**Figure S2A**): outer layers including epidermis cortex, and a precursor of endodermis and cortex (ec pre); endodermal layers comprised of three distinct types (endo 1, 2, and 3); and the stele comprised of two main types along with a phloem type (stele phloem). Several traditional marker genes were used to facilitate annotation of root cell types (**Figure S2B-D**), as were marker genes identified in previous scRNA-seq studies (**Supplementary Table 3**). In general, scATAC marker genes did not show a strong overlap with RNA-based marker genes. Endodermis cells were an exception, as several of their scATAC marker genes (AT3G32980, AT1G61590, AT1G14580, AT3G22600, AT5G66390) were also found to be marker genes in single-cell RNA-seq studies.[24] While this lack of overlap makes annotation more challenging, it is consistent with the reported weak correlation of chromatin accessibility with gene expression.[23,25] Moreover, the finding that expression levels are not precisely predicted by nearby accessible sites suggests that accessibility can add orthogonal information about cell identity to further stratify cell types into distinct sub-types.

Sequences motifs of transcription factor families associate with cell type-specific sites of open chromatin

Accessibility at regulatory sites is driven by transcription factor binding and modification of local chromatin.[26] We examined if any of the cell type-specific accessible sites were associated with the presence of transcription factor binding motifs. To do so, we used a set of representative motifs for all *A. thaliana* transcription factor families and nearly every individual transcription factor[27] to tally these motif counts within all 21,889 peaks in the full scATAC-seq dataset to build a peak-by-motif matrix. As each peak can be described in terms of its relative accessibility in each of the identified cell types, we performed a linear regression for each motif to test for

significant association of accessibility and motif presence. Relative accessibility values were calculated by first pseudo-bulking all peak counts by cell type and then normalizing these cell type-specific peak accessibility scores to a background peak accessibility of all cells pooled together. By testing the association of motif counts and cell type-specific accessibility, we identified transcription factor binding motifs whose presence was correlated with higher accessibility in each cell type. However, because motif sequence content for individual transcription factors is redundant, we computed means across each transcription factor family.

We found significant associations with motifs from at least one transcription factor family in all cell types (**Figure 1D**). For example, relative chromatin accessibility in epidermal cells was strongly associated (q-values ranging from 1e-24 to 1e-133) with the presence of motifs from the WRKY transcription factor family; this family includes *TTG2*, which, along with *TTG1* and *GL2*, has important roles in atrichoblast fate in the epidermis.[28] Furthermore, the effects of each motif family on relative accessibility was sufficient to hierarchically cluster cell types according to broad tissue classes (**Figure 1D**). Based on similarities in motif associations, hierarchical clustering grouped all stele clusters (1, 2, and 11), epidermis and cortex (clusters 0 and 3), two endodermis clusters (4 and 10), and another endodermis cluster with epidermal precursor cells (clusters 7 and 8). That motif associations alone can distinguish among clusters and group similar ones together provides independent verification of the cell type-specific nature of the chromatin-accessible sites detected in the scATAC-seq data.

Integration of scATAC-seq and scRNA-seq data improves cell type annotation

Because scATAC-seq data both identified known root cell types and provided novel cell identity assignments not identifiable through scRNA-seq, we addressed whether combining these two datasets results in additional insights than what could be gained from either alone. We first addressed whether both data types could be embedded in the same low-dimensional space in a manner that maintains the cell identities defined by both scATAC-seq and scRNA-seq. Such embedding assumes that the underlying cell identities represented in each dataset are similar. Although the root tissue sampled for our scATAC-seq experiment was not identical to that used in previous scRNA-seq experiments, we expected that the same major cell types were sampled in both experiments. Moreover, the data generated by both methods share "gene" as a feature, *i.e.* accessibility near or within a given gene; expression of a given gene.

We used the anchor-based multimodal graph alignment tool from the Seurat package to find nearest-neighbor scRNA-seq matches for each cell in the scATAC-seq data.[29,30] In short, the tool identifies representative features (shared "anchor" genes in our case) in each dataset and looks for underlying correlation structure of those

features to group similar cells in a co-embedded space. We plotted all cells within the resulting co-embedded space with cell type labels from each dataset separately. Cells derived from scRNA-seq and scATAC-seq experiments were well mixed (**Figure 2A**). Moreover, we found that cells of the same type were co-localized independent of the source data (**Figure 2B, 2C**), though some separation by data type was apparent, likely owing to the imputation step of dataset integration.[29] This result suggests that RNA and ATAC signals, which are only poorly correlated in bulk studies, are capable of grouping cell identities when determined in individual cells of a complex tissue. We further used this co-embedded space to refine our earlier manual cell type annotations by transferring labels of neighboring scRNA cells onto the scATAC cells (**Figure S3A, S3B**); while most of these labels matched, the greatest number of mismatches was seen in endodermis sub-type 1. The transferred labels matched our manual annotations, and, in the case of epidermal cells, allowed us to separate a single scATAC cluster into hair and non-hair cells (**Figure 2A, Figure S3A, S3B**). Furthermore, this co-embedded space was additionally used to transfer quantitative metrics and gene expression values derived from scRNA-seq data (**Figure S3C**). The three distinct scATAC clusters that were assigned an “endodermis” label with this approach are a striking example of scATAC data yielding, within a single cell type, greater stratification of “types” than the generally richer scRNA data.

Epidermal cell layers show increased levels of endoreduplication

In contrast to scRNA-seq data, scATAC-seq data can provide insight into DNA copy number and its impact on gene regulation. DNA copy number is of special relevance in the *A. thaliana* root, as each cell layer undergoes different rates of endoreduplication.[19] In a diploid cell, a single accessible locus tends to show 1 or 2 transposition events. In polyploid cells with higher DNA copy number, a single accessible locus could show 4, 8, or even 16 transpositions. Therefore, cells containing a large number of peaks with >1 transposition event are likely to represent endoreduplicated cells. To identify such cells, we classified each cell by the mean number of cuts it contained per peak and examined the distribution of this metric, accounting for differences in total UMI counts (see Methods), to draw a threshold above which cells were classified as likely endoreduplicated (**Figure S4A, S4B**). We found the expected trend of higher endoreduplication in the outermost cell files, with reduced prevalence in the stele (**Figure S4C**).

We then used a second method to identify endoreduplicated cells with a transcriptional signature. Instead of relying on the number of transpositions in the accessibility data directly, we instead leveraged the dataset integration described above (**Figure S3C**) to transfer scRNA-seq-based annotations to the cells in our scATAC experiment. To identify endoreduplicated cells in scRNA-seq data, we used a published set of marker genes for ploidy to generate signature scores for 2n, 4n, 8n and 16n ploidies.[19] With these scores, we predicted endoreduplicated cells by

calculating, for each cell, the ratio of the 8n signature relative to the diploid signature. Similar to the accessibility-based metric, this transcription-based approach identified endoreduplicated root cells in the expected pattern, with higher fractions in the epidermis cell layer and diminished levels in the stele (**Figure S4D, S4E**). We found these two methods of identifying endoreduplicated cells to be concordant (**Figure S4F**), but because the accessibility-based classification was less quantitative, we used the transcriptionally-based metric in subsequent analyses. This metric captured an abundance of tetraploid xylem cells in the stele (**Figure S4E**), consistent with previous findings.[19]

scATAC-seq captures three distinct endodermis types representing different developmental stages

We dissected the three endodermis clusters in greater detail using three approaches: (i) by identifying differentially accessible sites among sub-types; (ii) by aligning these sub-types to scRNA-seq data that have been annotated for endoreduplication and developmental progression; and (iii) by determining differentially expressed genes in the nearest-neighbors to each of these endodermis sub-types in scRNA-seq space (**Figure 3A**).

We identified few differentially accessible genes (adjusted p-value < 0.05 and at least 2-fold change in accessibility) in each endodermis sub-type: 25 for the first sub-type, 24 for the second, and 17 for the third (**Figure 3A**). The low number of associated genes precluded gene set enrichment analyses, but genes uniquely accessible in sub-type 1 included transcription factors *MYB85* (AT4G22680) and *NAC010* (AT1G28470) as well as genes involved in suberization (*FAR1*, *FAR4*, *FAR5*).[31] Endodermis sub-type 2 showed increased accessibility at *HIPP04* (AT1G2900), encoding a heavy metal-associated protein, *ANAC038* (AT2G24430), and phenylpropanoid metabolism genes.[32] Endodermis sub-type 3 showed strong accessibility at the *BLUEJAY* (AT1G14580) locus encoding a C2H2 transcription factor implicated in endodermis differentiation (**Figure 3B**),[33] as well as *MYB122* (AT1G74080) and other genes for phenylpropanoid biosynthesis (*PER22*, *PER32*, *PER72*, *BGLU32*).[32] We addressed whether these differentially-accessible genes show different expression patterns in endodermis cells in scRNA-seq space by mapping expression of each gene onto a subclustered set of endodermis cells combined from several scRNA-seq studies of the *A. thaliana* root.[2–6] The small set of marker genes identified for each scATAC sub-type showed no consistent expression pattern in the scRNA-seq data (**Figure S5A**), suggesting that other features distinguished these three sub-types.

Structure within two-dimensional embeddings of scRNA-seq and scATAC-seq data derived from developing tissues is often associated with differences in developmental progression or other asynchronous processes like the cell cycle. Furthermore, root tissue has the unique feature of being highly endoreduplicated,

which could also account for differences among the sub-types. To assess whether the endodermal sub-types were associated with these features, we added annotations for, developmental progression, endoreduplication and cell cycle to the combined root scRNA-seq data and used data integration (as in **Figure 2**) to test whether cells from the endodermal sub-types were associated with any of these features (**Figure S3C**).

We assessed developmental progression with two orthogonal methods: (i) correlation with published bulk expression data taken along longitudinal sections of the root;[1] and (ii) a modified measure of loss in transcriptional diversity (see Methods), which correlates strongly with developmental progression in a large number of scRNA-seq datasets, including of the *Arabidopsis* root.[2,34] We found that the developmental progression metric as measured by loss in transcriptional diversity was strongly associated with the orthogonal correlation-based classification in cells derived from scRNA-seq alone (**Figure S5B**).[34] For each cell of the endodermal sub-types, we calculated the average developmental progression of its 25 nearest neighbors among root scRNA-seq cells (**Figure S5C, S5D** and found, assigning this average to each scATAC endodermis cell, a trend of developmental progression among the endodermis sub-types (**Figure 3C**). This result was robust to changes in the number of neighbors used to identify similar cells from scRNA-seq data (**Figure S5E)**. This trend was the same if we calculated the developmental progression metric based on scATAC-seq data alone (**Figure S5F**), though the correlation to the transcriptional metric was weak overall (**Figure S5G**).[34] Cells from sub-type 1 were the least developed, while cells from sub-type 3 tended to co-occur with the most mature endodermal cells in the co-embedded graph (**Figure 3C**). We conclude that the three endodermal sub-types primarily represent cells of differing developmental progression and that differences in chromatin accessibility are able to capture this stratification of endodermis maturity.

Developmental progression in the root is associated with increased ploidy through endoreduplication.[19] Using the transcriptional-based metric for endoreduplication described above, we examined the predicted ploidy of orthogonally-classified cells derived from scRNA-seq (**Figure S5H**) and from the nearest RNA-seq neighbors of each endodermis sub-type (**Figure S5I**). We found that the younger endodermis sub-type 1 cells had mostly 2n neighbor cells, while the more mature sub-types 2 and 3 had mostly endoreduplicated neighbor cells, with similar levels in each (**Figure 3D**).

To better understand the differing transcriptional and chromatin accessibility patterns among endodermis sub-types, we analyzed differentially expressed genes from each endodermis sub-type. The early endodermis type, which is not yet endoreduplicated, showed an enrichment of genes (**Supplementary Table 4**) involved in Casparian strip formation (*CASP3*, *CASP5*) and wax biosynthesis (HHT1). The intermediate sub-type 2 also showed enrichment for genes involved in Casparian strip formation (*CASP3*, *CASP4*, *CASP5*, *GSO1*), as well as mechanosensitive ion channels

(*MSL4*, *MSL6*, *MSL10*) (**Supplementary Table 5**). The most advanced endodermis sub-type 3 showed enrichment for stress responses and metabolism of toxic compounds, kinase activity, and aquaporin water channels (**Supplementary Table 6**), consistent with this mature endodermis cell type modulating water permeability via aquaporins as well as through suberization.[35] We also identified putative regulators of these stages by looking for transcription factors among the genes that showed specificity for each endodermis cluster. The earlier endodermis type showed a single upregulated transcription factor, ERF54, while the intermediate sub-type showed 14 upregulated transcription factors, including *KNAT7*, *SOMNUS*, and *HAT22*. *MYB36*, which was found expressed in the later endodermis type, activates genes involved in Casparian strip formation and regulates a crucial transition toward differentiation in the endodermis.[36] Because *MYB36* regulates early steps of endodermis differentiation,[3,36] this result suggests that some more mature endodermis types may be absent in these data, perhaps due to technical differences in their ability to be lysed during nuclear extraction (see Methods).

We used a list of known cell-cycle marker genes (Arabidopsis.org) to generate a signature score marking proliferating cells. This signature score identified cycling cells in other cell types, such as early epidermis cells near the quiescent center (**Figure S6A, S6B**) in a meta-analysis of previously published scRNA-seq data. However, when this signature score was transferred to the scATAC-seq endodermis clusters by the nearest neighbor procedure described in Figure S3C, we observed no differences corresponding to each endodermis sub-type (**Figure S6C**). We conclude that cell cycle does not distinguish the endodermis sub-types.

Overall, the combined information gained from transcriptional signatures of developmental progression and endoreduplication highlights the importance of integrating both open chromatin and transcriptional profiling to identify cell types or cell states that may have otherwise been obscured in a single data type.

Predicting regulatory events using integrated scRNA and scATAC data

We previously identified transcription factor binding motifs that were enriched at cell type-specific peaks in the root (**Figure 1D**). While individual motifs may be associated with binding and activation by transcription factors, a sequence-level analysis cannot distinguish among the many members of plant transcription factor families that share near-identical sequence preferences. For example, WRKY family motifs were highly enriched among epidermis and cortex accessible sites, but this family contains >50 individual genes. In order to narrow down this list of genes to a few possible candidates, we leveraged our nearest-neighbor annotation approach (**Figure S3C**) to examine expression levels of all WRKY family transcription factors in the scATAC data (**Figure 4A**). Overall, we found that the majority of WRKY members showed expression in the epidermis, cortex or epidermal precursor cells (**Figure 4A**),

388 though some members showed stele-specific expression. To identify the most likely
389 members to bind the abundance of motifs in epidermis-specific peaks, we ranked
390 these genes by their specificity in the epidermis. The top four most epidermis specific
391 genes, *WRKY75*, *WRKY9*, *WRK6*, and *TTG2* (**Figure 4A**), have documented roles in
392 root development.[28,37–39] *TTG2* showed strong specificity for the epidermis, but we also
393 predict expression in some cortex and precursor cells (**Figure 4B**). Two key interacting
394 factors of *TTG2* that also contribute to epidermis development, *GL2* and *TTG1*,[40,41]
395 showed epidermis expression and had correlated patterns (Pearson correlation with
396 *TTG2* across cells for *GL2* = 0.91, and *TTG1* = 0.47) across all cells (**Figure S7A, S7B**).
397
398 Given the important role of *TTG2* in specification of atrichoblast fate in the
399 epidermis, we examined the consequences of its expression on accessibility of
400 individual peaks. Inference of individual regulatory events, particularly those involving
401 transcription factors, has long been a goal of studies that profile accessibility at
402 regulatory sites in bulk tissue. The varied cell states revealed by single-cell profiling
403 data, even those within a cell type, allow higher-resolution inference of these events.
404 To identify accessible sites that showed altered accessibility as a function of
405 transcription factor expression, we used a linear regression approach. We identified
406 617 peaks that showed significant (q-value < 0.05) associations with *TTG2* expression
407 levels (**Supplementary Table 7**). To visualize these associations using scATAC data,
408 we pseudo-bulked epidermis, cortex, and c/e precursor cells into four equal-sized bins
409 based on their level of *TTG2* expression (**Figure 4C**). We observed peaks whose
410 accessibility increases (**Figure 4C**, top and lower-left panels) and decreases (**Figure**
411 **4C**, lower-right panel) in cells with increasing levels TTG2 expression. Most significant
412 associations were positive, such that increased *TTG2* expression led to increased peak
413 accessibility (**Figure 4D**). Using DAP-seq data for *TTG2*, we examined whether peaks
414 with either positive or negative associations contain *TTG2* binding sites.[27] Positive
415 associations occurred whether or not a WRKY binding motif was present in the
416 associated peak (**Figure 4C, 4D**), suggesting that the role of WRKY transcription
417 factors in specification of the epidermis likely requires both direct and indirect
418 regulatory events. Of peaks with significant (q-value < 0.05) positive associations with
419 *TTG2* expression, 80% of these contained a WRKY binding motif, while only 38% of
420 the peaks with negative associations contained a binding motif (**Figure 4D**). Overall,
421 this analysis identifies transcription factors and putative target sites that constitute
422 regulatory events important for specifying cell types; these genes and regulatory sites
423 are good candidates for further functional studies.
424
425 **Discussion**
426
427 By profiling chromatin accessibility in the *A. thaliana* root at single-cell
428 resolution, we assessed cell types, developmental stages, the transcription factors
429 likely driving these stages and DNA copy number changes. We assigned over 5,000
430 root cells to tissues and cell types, demonstrating that these assignments are

concordant with single-cell transcriptomic studies. These results answer an unresolved question in plant gene regulation: does the paucity of dynamic open chromatin sites seen in bulk profiling experiments represent an accurate reflection of uniform gene regulation in *A. thaliana* or does it reflect a confounding effect of bulk studies? We found that distinct root cell types show unique patterns of open chromatin sites, with approximately 1/3 of all accessible sites showing cell type-specific patterns. This estimate greatly exceeds the earlier estimates from bulk studies of only 5-10% of accessible sites showing tissue- or condition-specificity,[9] presumably due in part to tissue heterogeneity.

Although this single-cell ATAC study discovered many more dynamic accessible sites, the correlation between dynamic accessibility and gene expression in single cells remained poor, reminiscent of the equally poor correlation seen in bulk studies. These data types would be integrated more faithfully in a true co-assay experiment.[25,42] Technical differences in nuclei versus cell-based assays, size selection, developmental stage, and sequencing depth may also contribute to differences between scRNA and scATAC datasets. While increasing the depth of our ATAC signal per cell may alleviate some of this noise, we argue that the poor correlation between chromatin accessibility and gene expression is not a function of data quality. Instead, we propose that this weak correlation reflects the complex nature of regulatory processes underlying development, and the differential aspects of regulation captured in scATAC-seq and scRNA-seq data, which were notably divergent in the scATAC-specific endodermis sub-types. Although the correlation of chromatin accessibility and gene expression is weak at the level of individual loci, either the entirety of a cell's regulatory landscape or its transcriptome can independently capture its cell identity. It is this feature that allows joint co-embedding of both data types and the use of scRNA-seq data to annotate scATAC cells.

Thus, while the patterns of both chromatin accessibility and gene expression contain information on cell identity and development, the relationships between these patterns are not well-ordered or parsimonious. For the many cells belonging to a distinct cell type, gene expression results from direct and indirect regulatory events involving tens or hundreds of transcription factors and chromatin remodelers that do not necessarily act in concert. For any individual locus, then, the expectation that average accessibility predicts average expression breaks down. Without a simple one-to-one model to explain regulatory output, we are left with significant heterogeneity within and between cell types, and a subset of convergent expression or accessibility patterns that define cell type specificity. Alternative explanations for the discrepancy in accessibility and expression include: (1) maintenance of cell identity requires that a cell's accessibility and expression profile stably reflect the convergent pattern for that cell type only a fraction of the time; and/or (2) cells have multiple accessibility and expression patterns that are sufficient to maintain cell identity and together constitute the convergent patterns we observe. In both scenarios, the heterogeneity in cell type specification will be buffered by factors outside chromatin accessibility or gene

expression, such as spatial location in tissue, metabolic determinants of cell function or developmental age.

We posit that scATAC-seq data combined with scRNA-seq data will ultimately resolve these alternatives by enabling mechanistic models of gene regulatory networks. scATAC-seq data alone are sufficient to identify the full set of accessible sites in the *Arabidopsis* genome, and examination of the transcription factor motifs within these sites can enable predictions of regulatory networks. However, many plant transcription factor families are large, some containing over fifty members that recognize near identical motifs. Thus, the accessibility data must be integrated with single-cell expression data that capture cell type-specific expression of transcription factors in order to narrow down the most probable transcription factors that are enacting individual regulatory events. The simple regression framework provided in this work is only a small step toward more complicated models that capture other relevant sources of heterogeneity. Building higher resolution models of key regulatory events will require the expression level of individual transcription factors in a cell type, the accessibility of individual peaks in this cell type and the presence of binding motifs corresponding to the relevant transcription factors. Theoretically, a comprehensive capture of cell states with both open chromatin and transcriptional profiling will allow the ordering of gene regulatory events and the larger scale ordering of regulatory programs that underlie development. The ability to take single-cell measurements over distinct developmental stages will also increase the sampling of key regulatory events. Ultimately, achieving the goal of building models of gene regulatory events underlying development will require ever larger datasets to fully capture the range of possible cell states.

In the future, single-cell studies of more complex plant tissues in crops and other species will necessitate larger numbers of profiled cells and higher numbers of cuts per cell. Deeper coverage in future datasets should enhance our ability to detect rare cell types and more confidently predict copy number from accessibility data alone. In this way, approaches that maximize the number of cells profiled at low cost, such as single-cell combinatorial indexing,[43] will be critical. Annotation in future studies will also present a substantial challenge if a rich literature and genomic analyses, including single-cell transcriptome profiles, are not available. Nevertheless, as shown in this proof-of-principle study of the well-characterized *A. thaliana* root, the knowledge gained should eventually allow us to manipulate gene expression and organismal phenotype in a targeted manner.

Methods

Plant Material

Genotype: *Arabidopsis thaliana* ecotype Col-0 INTACT line *UBQ10*:NTF::*ACT2*:BirA (available from ABRC, stock CS68649). *Growth conditions*: LD (16h light/8h dark), 22C,

519 ~100 µmol m2s, 50% RH. *Sample*: whole roots, harvested 12 days after germination,
520 from seedlings grown vertically on MS + 1% sucrose, atop filter paper (to facilitate root
521 harvesting).
522
523 *Nuclei Isolation and scATAC-seq*
524 Nuclei were isolated following a modified version of the protocol described in Giuliano
525 *et al*., 1988, as follows: 1g of roots was split in two batches of 0.5g, and each batch
526 chopped with a razor blade in 1 ml of Buffer A (0.8M sucrose, 10mM MgCl2, 25mM
527 Tris-HCl pH 8.0 and 1x Protease Inhibitor Tablet).[44] Extracts were combined, final
528 volume increased to 5ml with Buffer A, and incubated on ice for 10min, with gentle
529 swirling. The combined extract was filtered through miracloth, passed through a 26ga
530 syringe five times and re-filtered through a 40um cell strainer (BD Falcon). After
531 centrifugation at 2,000g 5min, the pellet was resuspended in 1ml Buffer B (0.4M
532 sucrose, 10mM MgCl2, 25mM Tris-HCl pH 8.0, 1x Protease Inhibitor Tablet, 1% Triton
533 X - 100) and loaded atop a 2-step 25/75 Percoll gradient (1 volume 25% Percoll in
534 Buffer B over 1 volume 75% Percoll in Buffer B). After centrifugation at 2,500g for
535 15min, nuclei were collected either at the 25/75 interface or in the subjacent 75
536 fraction, washed with 5 vols of Buffer B and recovered by centrifugation at 1,700g for
537 5min. The nuclei pellet was resuspended in 100ul Buffer B + 1% BSA and any nuclei
538 clumps broken down by pipetting up and down multiple times. Nuclei yield with this
539 protocol was ~ 94,000 nuclei per gram of roots (fresh weight).
540 scATAC-seq libraries were built using the 10x Genomics Chromium Single Cell ATAC
541 Solution platform, following manufacturer's recommendations. Before transposition,
542 nuclei were spun 5min at 1,500g and resuspended in 10x Genomics Diluted Nuclei
543 Buffer, at a concentration of 3,200 nuclei/ul. 5ul of nuclei suspension were used for
544 transposition (16,000 nuclei being the maximum input recommended for 10x
545 Chromium, and 10,000 nuclei being the expected recovery).
546
547 *Combining and processing of root scRNA-seq data*
548 Samples were processed using the CellRanger v1.2.0 pipeline from 10X Genomics,
549 including updated filtering of "halflet" cells that emerge due to multiply-barcoded
550 droplets.
551
552 *Integration of scRNA and scATAC data*
553 The R package Seurat version 3.1.5 was used to align and co-embed the scATAC-seq
554 data with scRNA-seq data published by Ryu et al. 2019, and to transfer cell type labels
555 from the scRNA data to the scATAC data.[30,45]
556
557 The standard workflow and default parameters as described in the Seurat vignette
558 "PBMC scATAC-seq Vignette" (satijalab.org/seurat/v3.1/atacseq_integration_vignette)
559 were used with the exception that all features (genes) were used when identifying
560 transfer anchors and performing the co-embedding rather than a set of "variable"
561 features as used in the vignette. Briefly this workflow is as follows:

An anchor set was established with the function FindTransferAnchors() linking the two datasets. Cell type annotations were transferred from the scRNA-seq data to the scATAC data using the function TransferData(). Imputed RNA-seq count data was generated for the scATAC cells, again using the TransferData() function. The imputed RNA data was then merged with the true scRNA-seq dataset and embedded in 2D UMAP space using Seurat functions.[29]

A co-embedding was performed with a super-set of previously pubished scRNA-seq data.[2,3,5] In the co-embedded space the scATAC-seq were found to be most closely co-located with data from root tips.[5] Based on this observation co-embedding was performed with solely with root tip dataset.[5]

Nearest neighbor analysis for transcriptional characterization of cells identified in scATAC assay

To annotate cells from the scATAC-seq assay with transcriptional features, we used average feature values from the nearest RNA neighbors in our co-embedded data (**Figure 2A**). In short, the 'distances' package in R was used to extract cell labels for the 25 nearest neighbors of each scATAC cell. For a feature of interest (individual gene expression, cell-cycle signature score, endoreduplication signature score, developmental progression signature), we calculated the mean expression from the 25 scRNA cells, and assigned that mean score to each ATAC cell (**Figure S3C**).

Endoreduplication signatures

We identified endoreduplicated cells using two different approaches, the first using scRNA data, and the second using scATAC data. In the first approach (as in **Figure 3D**, **Figure S4D, S4E, Figure S5B, S5I**), validated sets of endoreduplication markers for 2N, 4N, and 8N cells were used to identify endoreduplicated cells in the scRNA data.[19] We used the nearest neighbor approach described above to transfer this transcriptional signature to scATAC cells. The average expression of each gene group was computed for each individual cell, and subsequently averaged per cluster to generate cell type-specific levels of each ploidy signature. To identify clusters that were more likely to be endoreduplicated, rather than typical diploid cells, we examined, for each cluster, the ratio of the endoreduplicated signatures (4N or 8N) relative to the diploid (2N) signature. Clusters with a higher ratio are more likely to represent endoreduplicated cells. In the second approach (as in **Figure S4A-C**), the number of transposition events derived from scATAC data were used directly to identify endoreduplicated cells. We assumed that cells containing higher than average cuts per peak were more likely to be endoreduplicated, as the cut counts for a single peak in a diploid cell should rarely be above two. A peak with a cut count >2 may indicate an extra copy of the locus present in that cell. To identify cells more likely to be endoreduplicated, then, we examined the distribution of cuts per peak for all cells, but

found this metric was strongly correlated with total UMIs per cell. To account for contribution total UMIs per cell, we used the relationship between the cuts/feature and total UMIs per cell to compute a Loess model fit (**Figure S4B**). We then used residuals of this model as a metric to identify cells that have higher cuts/feature than would be expected based on their total UMIs. We set an arbitrary threshold of >1 SD in the distribution of each cell's deviation from the fit line, and defined endoreduplicated cells as those beyond the threshold (**Figure S4B**). For each cell, a binary designation of endoreduplication was applied based on whether the cell crossed this threshold.

Transcriptional diversity metric for developmental progression

Using the general premise that the number of unique genes expressed (transcriptional complexity) tends to be reduced across the developmental trajectory of a cell type as it moves from earlier to later stages,[13] we devised a metric to approximate relative differences in developmental progression among cells. Measuring the number of unique genes expressed is distinct from measuring the number of UMIs or transcripts captured per cell, which can vary across cell types. To account for differential recovery of UMIs across cells in the transcriptional complexity measure, we modeled as a Loess fit the relationship between total UMIs captured and the number of unique genes expressed per cell. With this fit, we identified cells that have many more or fewer unique genes expressed than would be expected for cells over a range of captured UMIs. Developmental progression for each cell was defined as the residual of each point in this fit, allowing separation of earlier cells (more unique genes expressed than would be expected for a given number of captured UMIs) from later cells (fewer unique genes expressed than would be expected for a given number of captured UMIs).

Motif analysis

Position weight matrices from the comprehensive DAP-seq dataset[27] were used as input into FIMO[46] to search for significant matches for each individual TF motif (adjusted p-value threshold < 1e-5) in each of the scATAC peaks. With the output of this motif scan, we generated a matrix that tallied counts of each individual motif within each peak. Each individual motif in the DAP-seq dataset[27] has an associated TF family, and the counts per peak were averaged by family. To identify motifs whose counts were significantly associated with cell type-specific accessibility, we first generated, for each peak, a relative accessibility score by taking the mean accessibility of that peak in each cell cluster relative to the overall accessibility of that peak in all clusters. Next, we used a linear regression framework within Monocle3[47] to identify individual motifs whose counts showed strong positive or negative correlations with the cell type-specific accessibility score in each cell cluster. The effect size of each motif's contribution to cell type-specific accessibility is given as the β of the linear regression, shown as a mean across all transcription factors in the same family.

Data Availability

An R object containing all accessibility and predicted expression data for each cell has been deposited to Dryad (accession number pending).

Code Availability

We have provided R markdown files with code blocks sufficient to complete the primary processing of the data, generation of scATAC and scRNA co-embedding, analysis of motifs, and identification of transcription-factor mediated regulatory events. (Github repository link pending).

Acknowledgements

We thank Dr. Ken Jean-Baptiste and Dr. Kerry Bubb for valuable discussions on ATAC-seq analysis. We also thank Xavi Guitart for helpful discussions on endoreduplication. This work was supported by the National Science Foundation (RESEARCH-PGR grant 17488843) to S.F. and C.Q. This work was also supported by NIH grant 1RM1HG010461 to C.Q. and S.F and R01-GM079712 to C.Q. and J.C.

References

1. Brady, S. M. *et al.* A High-Resolution Root Spatiotemporal Map Reveals Dominant Expression Patterns. *Science (80-.).* **318**, 801–806 (2007).
2. Jean-Baptiste, K. *et al.* Dynamics of gene expression in single root cells of A. thaliana. *Plant Cell* **31**, tpc.00785.2018 (2019).
3. Shulse, C. N. *et al.* High-Throughput Single-Cell Transcriptome Profiling of Plant Cell Types. *Cell Rep.* **27**, 2241-2247.e4 (2019).
4. Zhang, T. Q., Xu, Z. G., Shang, G. D. & Wang, J. W. A Single-Cell RNA Sequencing Profiles the Developmental Landscape of Arabidopsis Root. *Mol. Plant* **12**, 648–660 (2019).
5. Ryu, K. H., Huang, L., Kang, H. M. & Schiefelbein, J. Single-cell RNA sequencing resolves molecular relationships among individual plant cells. *Plant Physiol.* **179**, 1444–1456 (2019).
6. Denyer, T. *et al.* Spatiotemporal Developmental Trajectories in the Arabidopsis Root Revealed Using High-Throughput Single-Cell RNA Sequencing. *Dev. Cell* **48**, 840-852.e5 (2019).
7. Sullivan, A. M. *et al.* Mapping and Dynamics of Regulatory DNA in Maturing Arabidopsis thaliana Siliques. *Front. Plant Sci.* **10**, 1–16 (2019).
8. Alexandre, C. M. *et al.* Complex relationships between chromatin accessibility, sequence divergence, and gene expression in arabidopsis thaliana. *Mol. Biol. Evol.* **35**, 837–854 (2018).
9. Sullivan, A. M., Bubb, K. L., Sandstrom, R., Stamatoyannopoulos, J. A. &

Queitsch, C. DNase I hypersensitivity mapping, genomic footprinting, and transcription factor networks in plants. *Curr. Plant Biol.* **3–4**, 40–47 (2015).

10. Reynoso, M. A. *et al.* Evolutionary flexibility in flooding response circuitry in angiosperms. *Science (80-.).* **365**, 1291–1295 (2019).
11. Maher, K. A. *et al.* Profiling of accessible chromatin regions across multiple plant species and cell types reveals common gene regulatory principles and new control modules. *Plant Cell* **30**, 15–36 (2018).
12. Saunders, L. M. *et al.* Thyroid hormone regulates distinct paths to maturation in pigment cell lineages. *Elife* **8**, (2019).
13. Gulati, G. S. *et al.* Single-cell transcriptional diversity is a hallmark of developmental potential. *Science (80-.).* **367**, 405–411 (2020).
14. Waddington, C. H. The Strategy of the Genes. (1959).
15. Orr-Weaver, T. L. When bigger is better: The role of polyploidy in organogenesis. *Trends Genet.* **31**, 307–315 (2015).
16. Derks, W. & Bergmann, O. Polyploidy in cardiomyocytes: Roadblock to heart regeneration? *Circ. Res.* **126**, 552–565 (2020).
17. Lang, L. & Schnittger, A. Endoreplication — a means to an end in cell growth and stress response. *Curr. Opin. Plant Biol.* **54**, 85–92 (2020).
18. Pirrello, J. *et al.* Transcriptome profiling of sorted endoreduplicated nuclei from tomato fruits: how the global shift in expression ascribed to DNA ploidy influences RNA-Seq data normalization and interpretation. *Plant J.* **93**, 387–398 (2018).
19. Bhosale, R. *et al.* A spatiotemporal dna endoploidy map of the arabidopsis root reveals roles for the endocycle in root development and stress adaptation. *Plant Cell* **30**, 2330–2351 (2018).
20. Robinson, D. O. *et al.* Ploidy and Size at Multiple Scales in the Arabidopsis Sepal. *Plant Cell* **30**, 2308–2329 (2018).
21. Blondel, V. D., Guillaume, J.-L., Lambiotte, R. & Lefebvre, E. Fast unfolding of communities in large networks. *J. Stat. Mech. Theory Exp.* **10**, P10008 (2008).
22. Shu, H., Wildhaber, T., Siretskiy, A., Gruissem, W. & Hennig, L. Distinct modes of DNA accessibility in plant chromatin. *Nat. Commun.* **3**, (2012).
23. Sullivan, A. M. *et al.* Mapping and dynamics of regulatory DNA and transcription factor networks in A. thaliana. *Cell Rep.* **8**, 2015–2030 (2014).
24. McFaline-Figueroa, J. L., Trapnell, C. & Cuperus, J. T. The promise of single-cell genomics in plants. *Curr. Opin. Plant Biol.* **54**, 114–121 (2020).
25. Cao, J. *et al.* Joint profiling of chromatin accessibility and gene expression in thousands of single cells. *Science (80-.).* **1385**, 1380–1385 (2018).
26. Spitz, F. & Furlong, E. E. M. Transcription factors: From enhancer binding to developmental control. *Nat. Rev. Genet.* **13**, 613–626 (2012).
27. O'Malley, R. C. *et al.* Cistrome and Epicistrome Features Shape the Regulatory DNA Landscape. *Cell* **165**, 1280–1292 (2016).
28. Johnson, Cameron S.; Kolevski Ben, and S. D. R. TRANSPARENT TESTA GLABRA2 , a Trichome and Seed Coat Development Gene of Arabidopsis,

Encodes a WRKY Transcription Factor. *Plant Cell* **14**, 1359–1375 (2017).

29. Stuart, T. *et al.* Comprehensive Integration of Single-Cell Data. *Cell* **177**, 1888-1902.e21 (2019).
30. Butler, A., Hoffman, P., Smibert, P., Papalexi, E. & Satija, R. Integrating single-cell transcriptomic data across different conditions, technologies, and species. *Nat. Biotechnol.* **36**, 411–420 (2018).
31. Domergue, F. *et al.* Three Arabidopsis fatty Acyl-coenzyme a reductases, FAR1, FAR4, and FAR5, generate primary fatty alcohols associated with suberin deposition. *Plant Physiol.* **153**, 1539–1554 (2010).
32. Raudvere, U. *et al.* G:Profiler: A web server for functional enrichment analysis and conversions of gene lists (2019 update). *Nucleic Acids Res.* **47**, W191–W198 (2019).
33. Moreno-Risueno, M. A. *et al.* Transcriptional control of tissue formation throughout root development. *Science (80-.).* **350**, 426–430 (2015).
34. Gulati, G. S. *et al.* Single-cell transcriptional diversity is a hallmark of developmental potential. *Science (80-.).* **367**, 405–411 (2020).
35. Kreszies, T., Schreiber, L. & Ranathunge, K. Suberized transport barriers in Arabidopsis, barley and rice roots: From the model plant to crop species. *J. Plant Physiol.* **227**, 75–83 (2018).
36. Liberman, L. M., Sparks, E. E., Moreno-Risueno, M. A., Petricka, J. J. & Benfey, P. N. MYB36 regulates the transition from proliferation to differentiation in the Arabidopsis root. *Proc. Natl. Acad. Sci. U. S. A.* **112**, 12099–12104 (2015).
37. Devaiah, B. N., Karthikeyan, A. S. & Raghothama, K. G. WRKY75 transcription factor is a modulator of phosphate acquisition and root development in Arabidopsis. *Plant Physiol.* **143**, 1789–1801 (2007).
38. Chen, Y. F. *et al.* The WRKY6 transcription factor modulates PHOSPHATE1 expression in response to low pi stress in arabidopsis. *Plant Cell* **21**, 3554–3566 (2009).
39. Zheng, X. *et al.* MdWRKY9 overexpression confers intensive dwarfing in the M26 rootstock of apple by directly inhibiting brassinosteroid synthetase MdDWF4 expression. *New Phytol.* **217**, 1086–1098 (2018).
40. Long, Y. & Schiefelbein, J. Novel TTG1 Mutants Modify Root-Hair Pattern Formation in Arabidopsis. *Front. Plant Sci.* **11**, 1–12 (2020).
41. Schiefelbein, J., Kwak, S. H., Wieckowski, Y., Barron, C. & Bruex, A. The gene regulatory network for root epidermal cell-type pattern formation in arabidopsis. *J. Exp. Bot.* **60**, 1515–1521 (2009).
42. Xing, Q. R. *et al.* Parallel bimodal single-cell sequencing of transcriptome and chromatin accessibility. *bioRxiv* 1027–1039 (2019). doi:10.1101/829960
43. Cao, J. *et al.* Comprehensive single-cell transcriptional profiling of a multicellular organism. *Science (80-.).* **357**, 661–667 (2017).
44. Giuliano, G. *et al.* An evolutionarily conserved protein binding sequence upstream of a plant light-regulated gene. *Proc. Natl. Acad. Sci. U. S. A.* **85**, 7089–7093 (1988).

45. Stuart, T. *et al.* Comprehensive Integration of Single-Cell Data Resource Comprehensive Integration of Single-Cell Data. *Cell* **177**, 1888-1902.e21 (2019).
46. Grant, C. E., Bailey, T. L. & Noble, W. S. FIMO: Scanning for occurrences of a given motif. *Bioinformatics* **27**, 1017–1018 (2011).
47. Cao, J. *et al.* The single-cell transcriptional landscape of mammalian organogenesis. *Nature* **566**, 496–502 (2019).

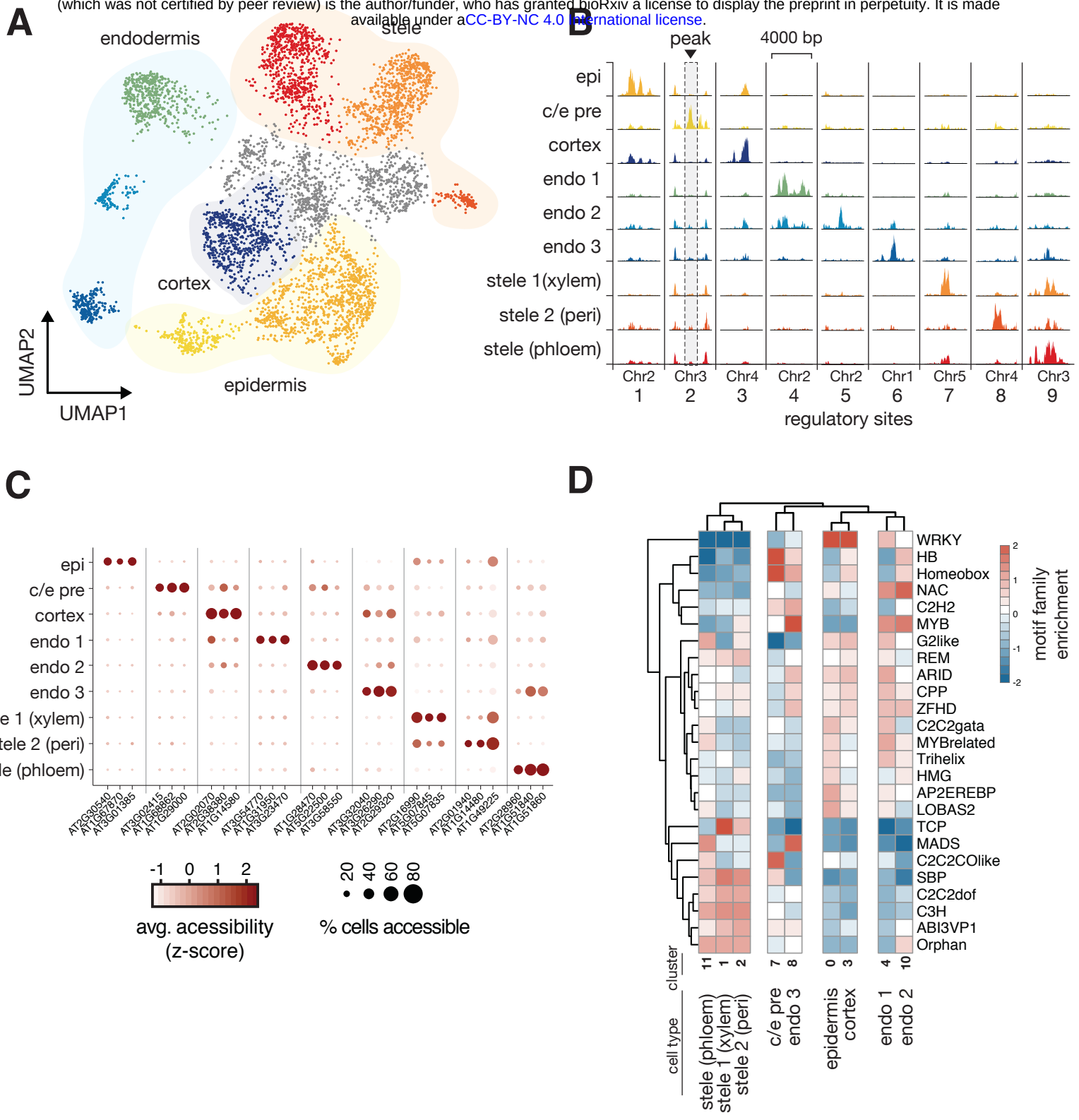

Figure 1. scATAC-seq identifies known root cell types.

Figure 1. scATAC-seq identifies known root cell types. (A) UMAP dimensionality reduction plot of root cells using peak-level scATAC data. Cells are colored according to Louvain clusters, and broad tissue types are indicated with transparent shading. (B) Pseudo-bulked peak tracks generated by combining ATAC data from all cells within a cluster. Each column represents a single locus in the genome that shows cell type-specific accessibility; each row represents a cell type, and each column shows an example marker peak for each type. Colors match those in previous panel. A cluster residing between the epidermis and endodermis clusters, with expression of markers from both cell types (**Figure S2B, S2C**) was given the label 'c/e pre' (precursor of cortex/endodermis, second row), and epidermis was shortened to 'epi'. (C) Dotplot showing marker genes for each cell type cluster. Each column represents a single gene's activity score, the summed accessibility of its gene body and promoter sequence (-400bp from transcription start site). The color of each dot indicates the magnitude of accessibility and the size of each dot represents the fraction of cells in each cell type showing accessibility at that gene. (D) Heatmap showing the predicted effect, across all peaks, of motifs from each *Arabidopsis* transcription factor family on cell type-specific accessibility. Darker shades of red indicate that presence of the motif is correlated with increased accessibility in that cell type, whereas shades of blue indicate that the motif is anti-correlated with accessibility. The mean effect all transcription factors within a given family are shown as rows, and each column represents a cell type.

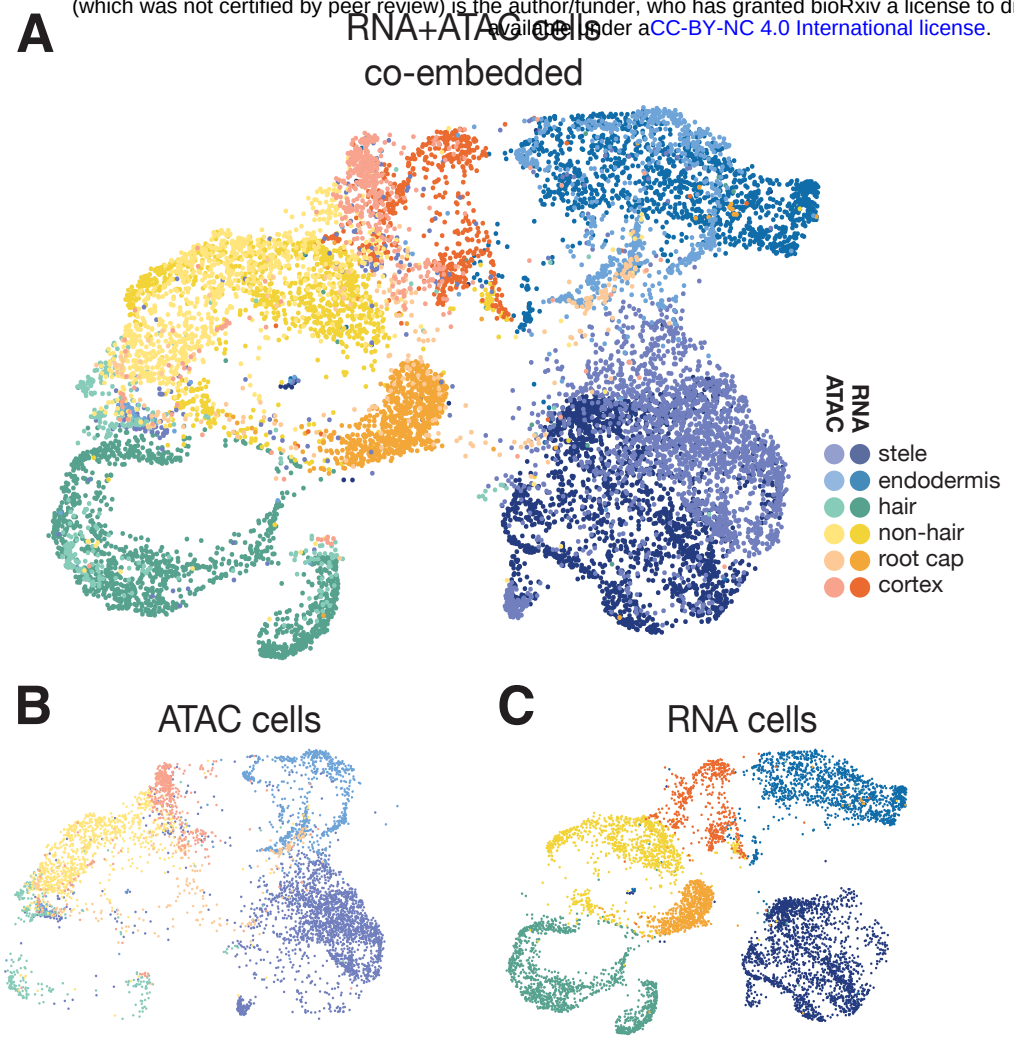

Figure 2. scATAC-seq data can be integrated with scRNA-seq data to identify cell types.

Figure 2. scATAC-seq data can be integrated with scRNA-seq data to identify cell types. (A) UMAP co-embedding of root scATAC cells alongside root scRNA cells.[5] Cells are colored by broad tissue type, with scATAC cells colored in lighter shades and scRNA cells in darker shades. (B) UMAP from (A), but showing only cells from the scATAC-seq experiment; (C) shows only cells from the scRNA-seq experiment.

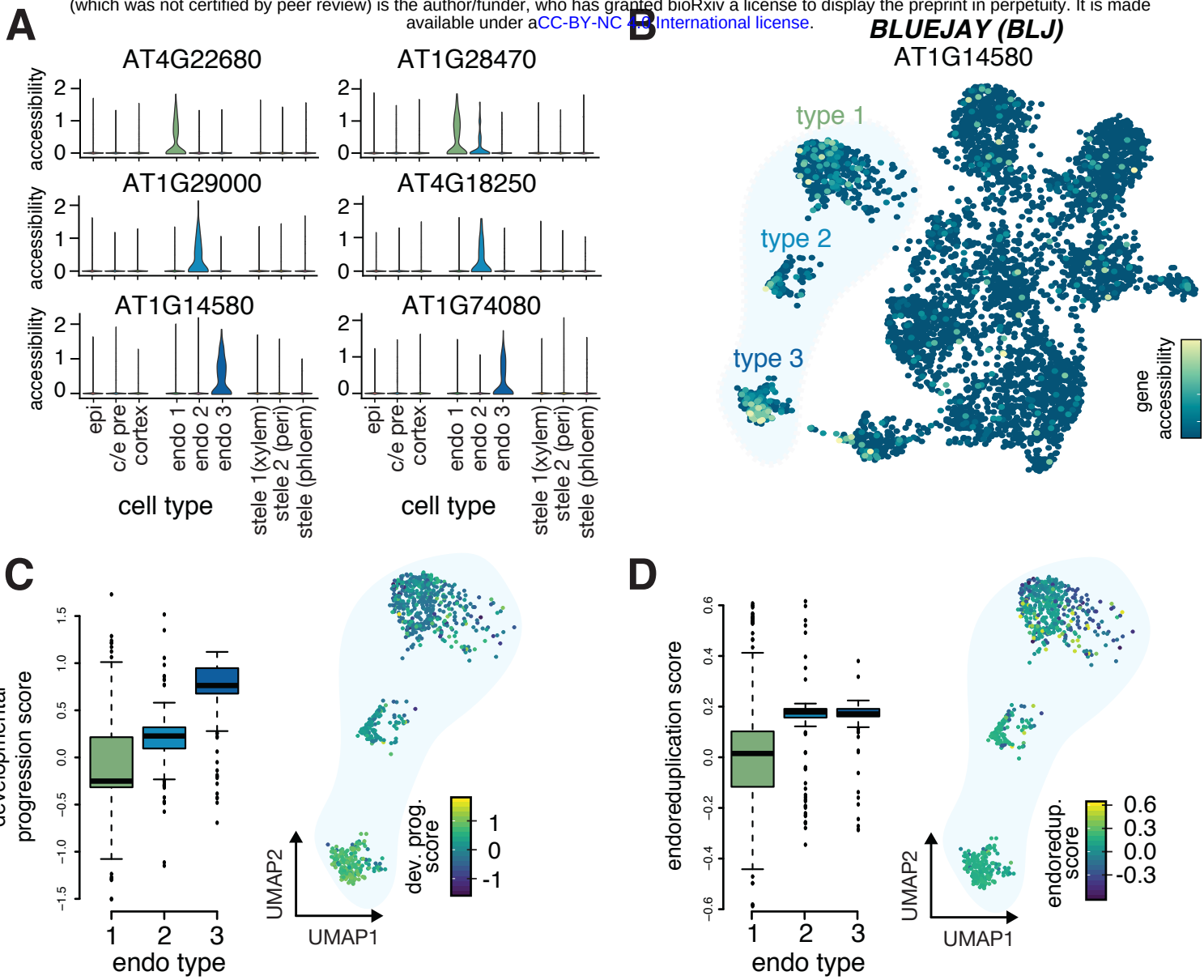

Figure 3. scATAC-seq identifies distinct sub-types of endodermal cells.

Figure 3. scATAC-seq identifies distinct sub-types of endodermal cells. (A) Violin plots showing specific patterns of accessible genes that mark each endodermal sub-type. Two examples are given for each endodermal sub-type, with gene-level accessibility scores indicated for all other cell types. (B) UMAP of all cells colored by accessibility of the *BLUEJAY* gene, which marks endodermal type 3; corresponding violin plot for this gene in lower left panel in (A). (C) Boxplot showing an increase in median developmental progression of each endodermal sub-type, as determined by average transcriptional complexity in the nearest 25 scRNA neighbors of each scATAC cell in the co-embedded representation from Fig. 2A; right inset shows UMAP of endodermal cells with each cell colored by the average developmental progression of its scRNA neighbors, mirroring the gradual increase seen in left panel. (D) Boxplot showing an increase in median levels of endoreduplication across endodermal sub-types, ascertained as in (C), but instead using a gene expression signature of endoreduplication; right inset shows UMAP of endodermal cells with each cell colored by the average endoreduplication score of its scRNA neighbors, with highest levels seen in endodermal sub-types 2 and 3.

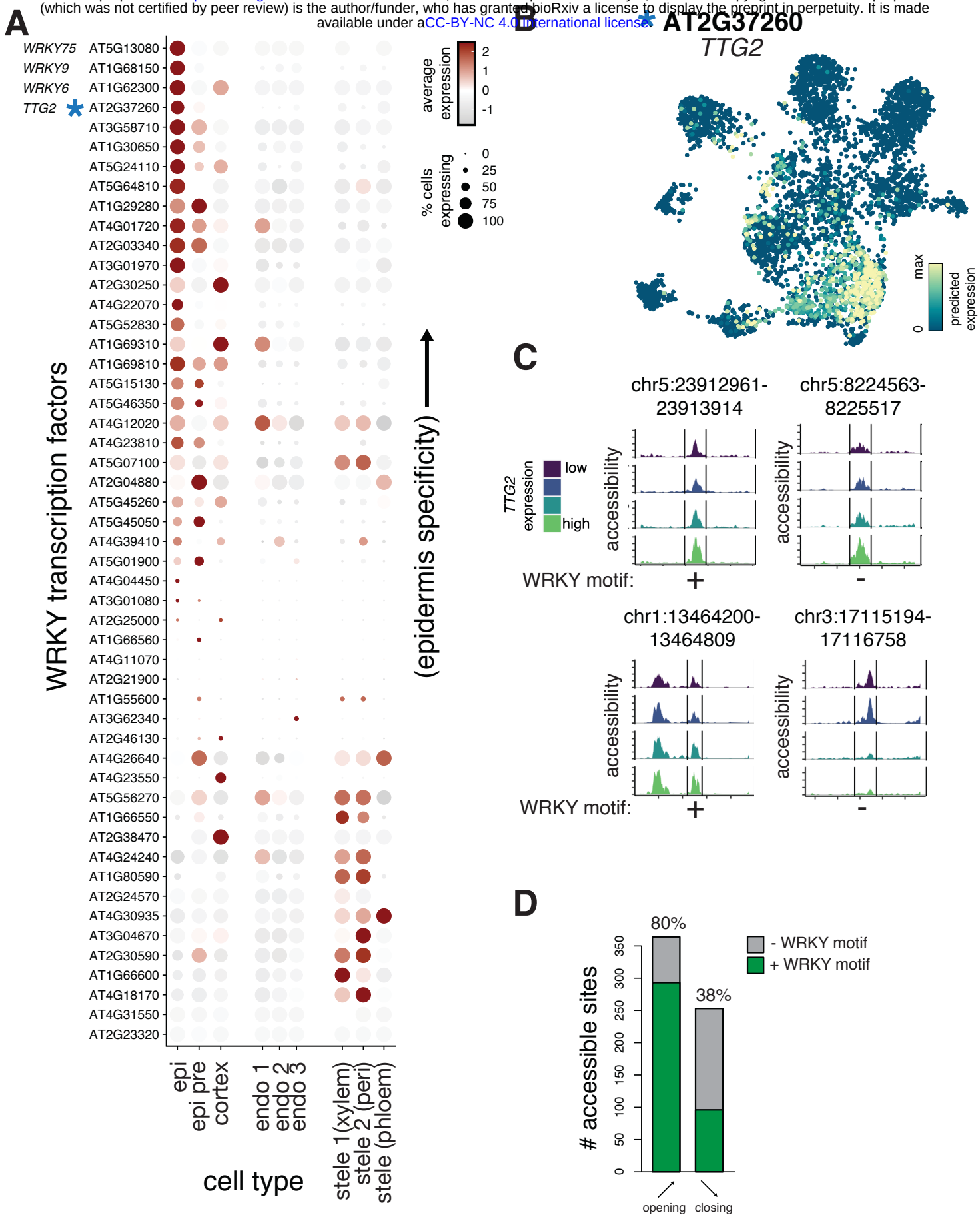

Figure 4. Prediction of candidate regulatory transcription factors from integrated scATAC and scRNA data.

Figure 4. Prediction of candidate regulatory transcription factors from integrated scATAC and scRNA data. (A) Dotplot heatmap showing predicted expression of all WRKY family transcription factors across all cells. The color of each dot indicates the magnitude of predicted expression of each gene and the size of each dot represents the fraction of cells in each cell type showing expression at that gene; genes (rows) are ordered by the specificity of their epidermis expression. (B) UMAP plot of cells derived from scATAC experiment, but colored by predicted expression of an epidermis-specific WRKY transcription factor, *TTG2*. (C) Pseudo-bulked accessibility tracks of epidermis peaks whose accessibility showed a significant association with predicted *TTG2* expression. Cells with higher *TTG2* expression are shown in lighter shades. All panels show examples of significant ($q < 0.05$) positive associations of *TTG2* expression with peak accessibility, with exception of the lower right panel. The presence or absence of a WRKY binding motif is indicated below each peak. (D) Barplot showing fraction of WRKY binding motifs in peaks of the epidermis, cortex, and pre-cursor type that showed significant association with *TTG2* expression. Peaks whose accessibility showed positive associations with expression are labelled as “opening”; those with negative associations are labeled as “closing.”

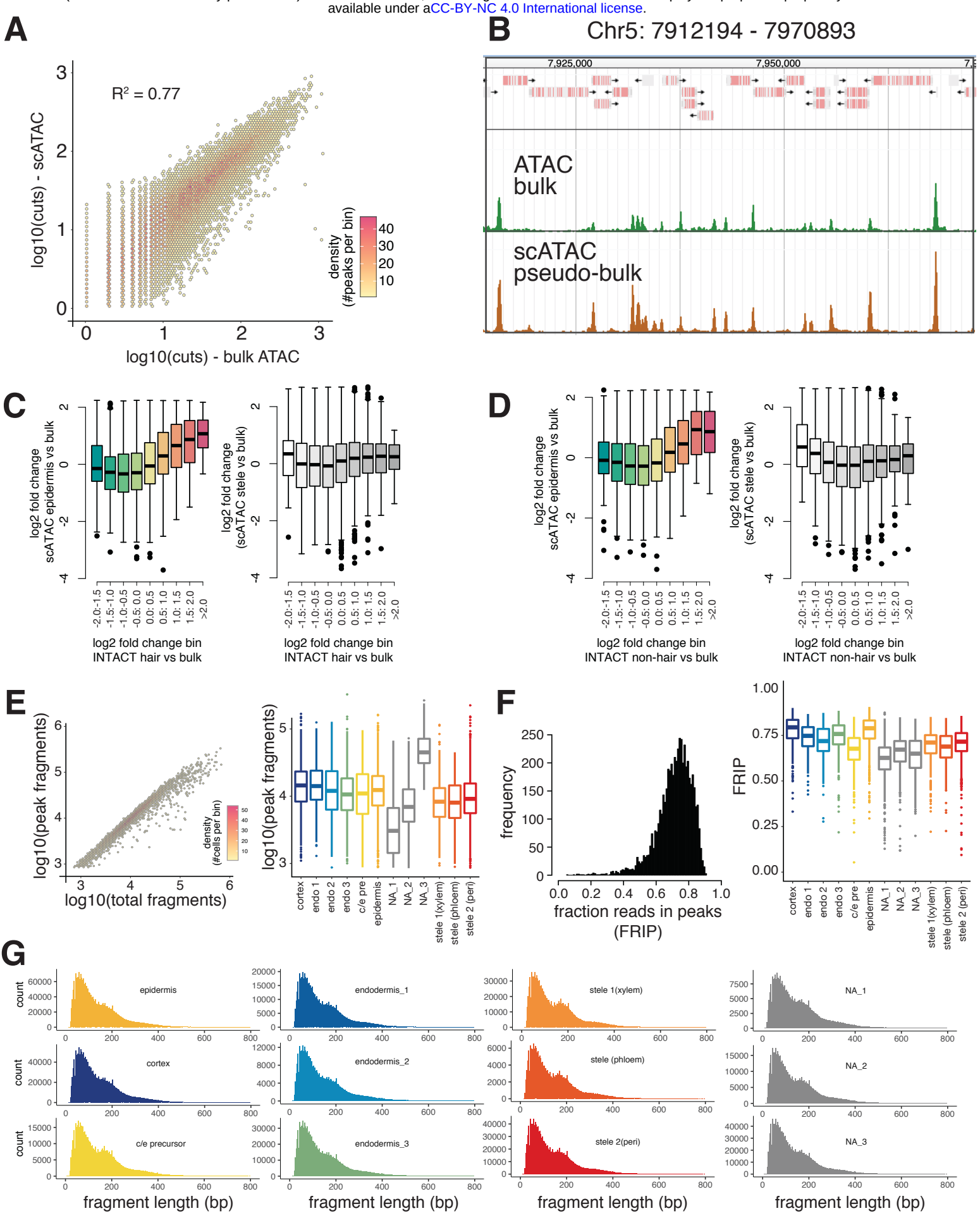

Supplementary Figure 1. Quality of scATAC-seq data is comparable to bulk ATAC-seq data.

Supplementary Figure 1. Quality of scATAC-seq data is comparable to bulk ATAC-seq data. (A) Scatterplot where each point represents peaks defined in the scATAC data. The x-axis shows the total cutcount within those peaks in bulk ATAC-seq and the y-axis shows the total cutcount within those peaks in scATAC-seq. Point density is indicated by increasing shades of red. (B) Example genomic region showing bulk ATAC accessibility (green) and pseudo-bulked scATAC accessibility (brown). Gene models are indicated above. (C) Boxplots showing peaks from scATAC assay in bins of increasing accessibility from an alternative, cell type-enriched ATAC approach;[11] peaks with low root hair cell-specific accessibility are in the leftmost bin, while those with the greatest root hair cell-specific accessibility are in the rightmost bin ($n > 300$ for all bins). Root hair-specific accessibility was defined as peak accessibility in INTACT-derived root hair cells relative to a bulk ATAC sample. The y-axis in the left panel denotes epidermis-specific accessibility determined from the scATAC experiment, defined by the accessibility of those peaks in epidermal cells relative to accessibility when all cell types are grouped (simulating a “bulk” sample). The y-axis in the right panel denotes the relative accessibility in stele cells as a control. (D) Identical to (C), except that peaks are grouped by relative accessibility in root non-hair cells, determined by an alternative cell type-enriched ATAC approach.[11](E) Read recovery per cell: Left panel shows relationship between total reads recovered per cell (x-axis) and reads in peaks (y-axis). Areas with higher point density are shown as in (A). Right panel shows boxplots of total number of reads in peaks recovered for each cell type. (F) ATAC quality per cell: Left panel shows the overall distribution of fraction of reads in peaks (FRIP) across all cells, right panel shows distribution of FRIP scores for each cell type. (G) Read length distributions for all fragments separated by cell type.

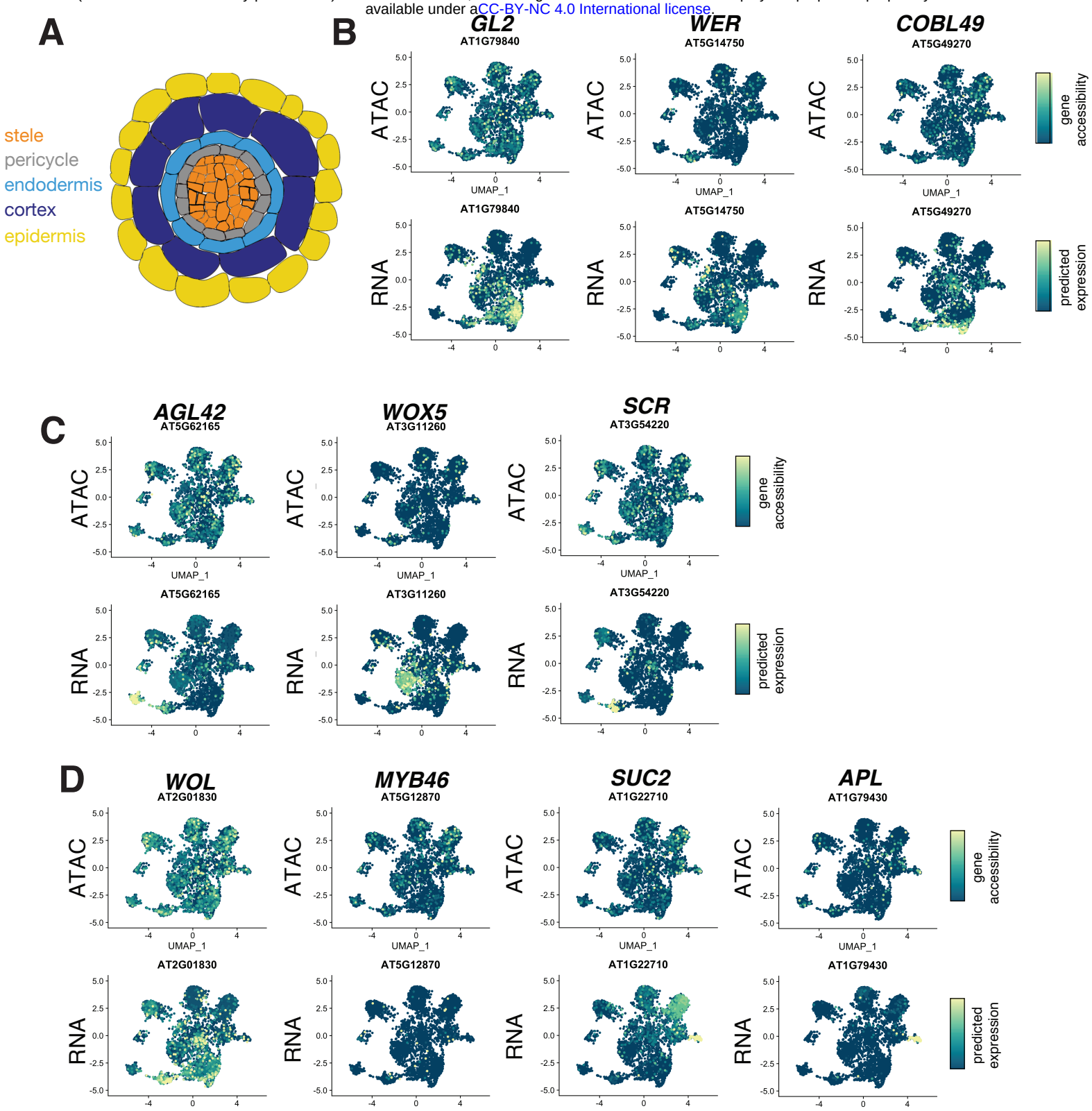

Supplementary Figure 2. Accessibility and predicted expression levels of traditional marker genes in major cell layers of the root.

Supplementary Figure 2. Accessibility and predicted expression levels of traditional marker genes in major cell layers of the root. (A) Schematic showing the major cell layers of the *Arabidopsis* root, colored as in Figure 1. (B) Marker gene plots for epidermis-specific genes showing accessibility (top) and predicted expression levels (bottom). Common and systematic gene names are indicated above. (C) As in previous panel, showing QC (*AGL42*), cortex (*WOX5*), and endodermis (*SCR*) markers. (D) As in previous panels, showing stele (*WOL* and *MYB46*) and phloem (*SUC2* and *APL*) markers.

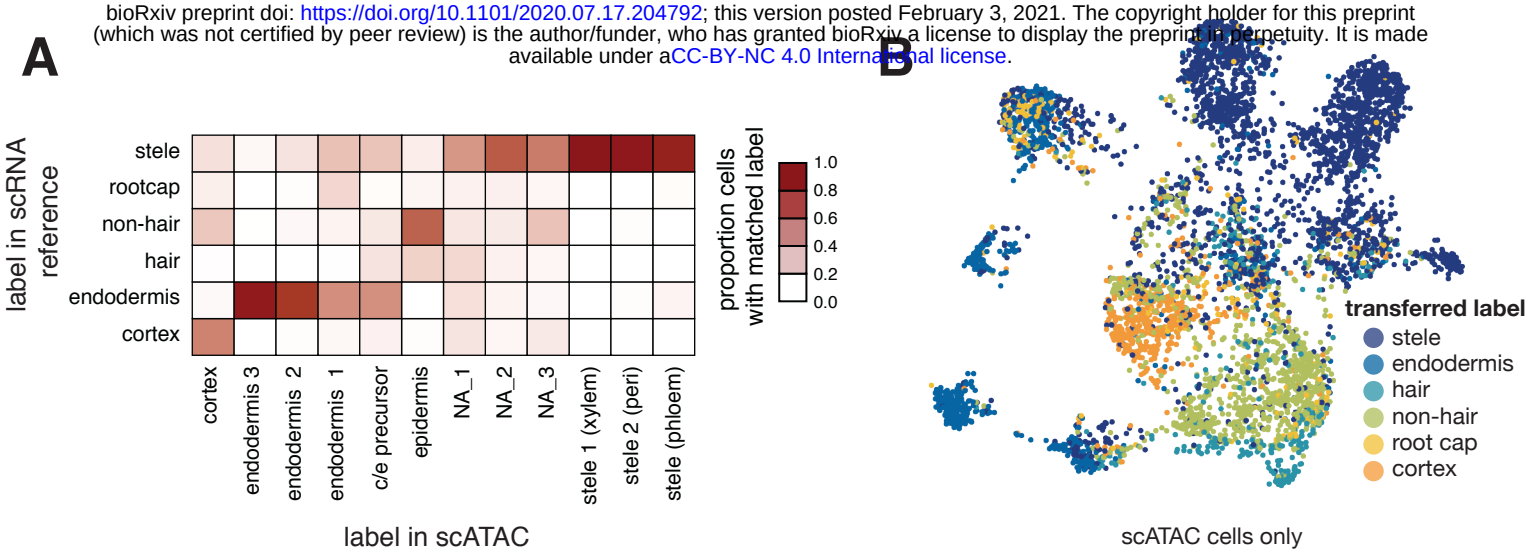

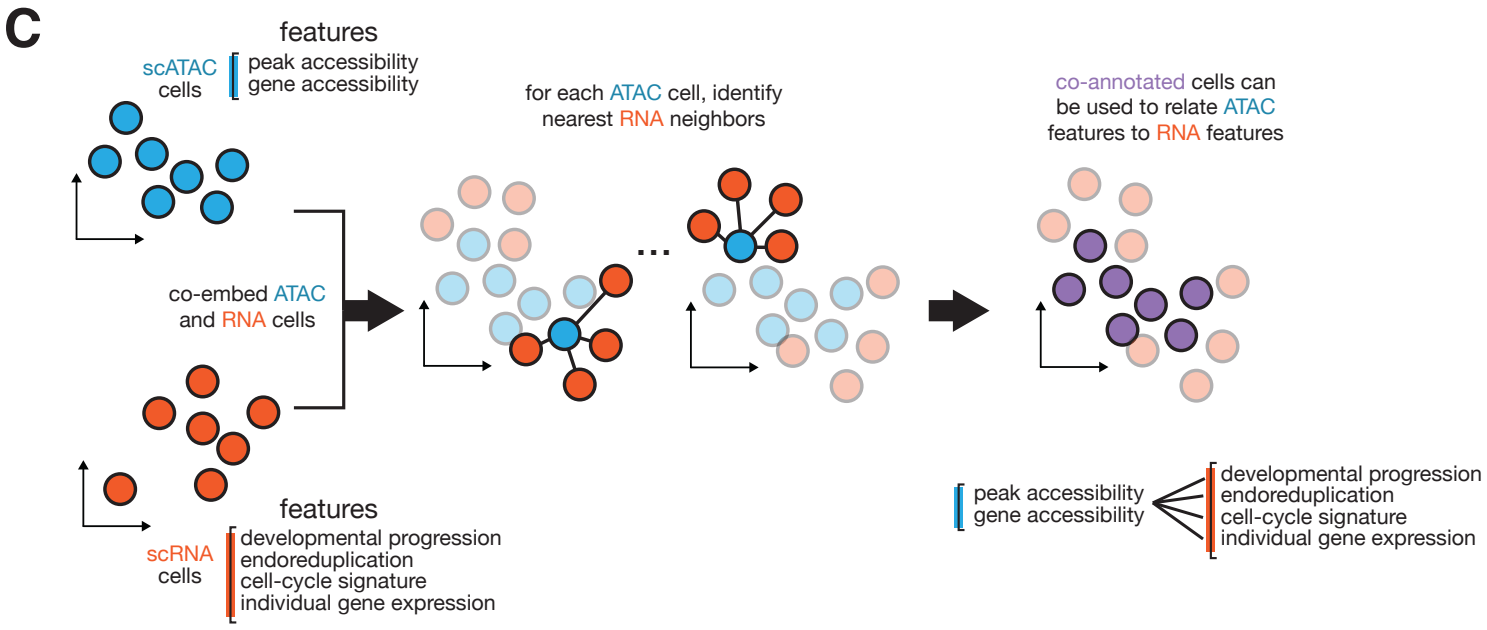

Supplementary Figure 3. Co-embedding of scATAC and scRNA data allows validation of cell type labels and annotation by RNA-derived features.

Supplementary Figure 3. Co-embedding of scATAC and scRNA data allows validation of cell type labels and annotation by scRNA-derived features. (A) Confusion matrix showing the correspondence of manual cell annotations (x-axis) with those derived from the label-transfer from RNA to ATAC cells (y-axis). (B) UMAP of scATAC cells as in Fig. 1A, but cells are colored by the cell type label predicted from annotations of scRNA nearest neighbors. These cell type labels broadly match those predicted by manual annotation, and separate the epidermis cluster into hair and non-hair cells. (C) Workflow schematic for annotation of scATAC-cells with transcriptional data. The 25 nearest RNA neighbors from each ATAC cell in the co-embedded graph (**Figure 2A**) were identified, and average expression of individual genes and signatures scores were computed and assigned to each scATAC cell.

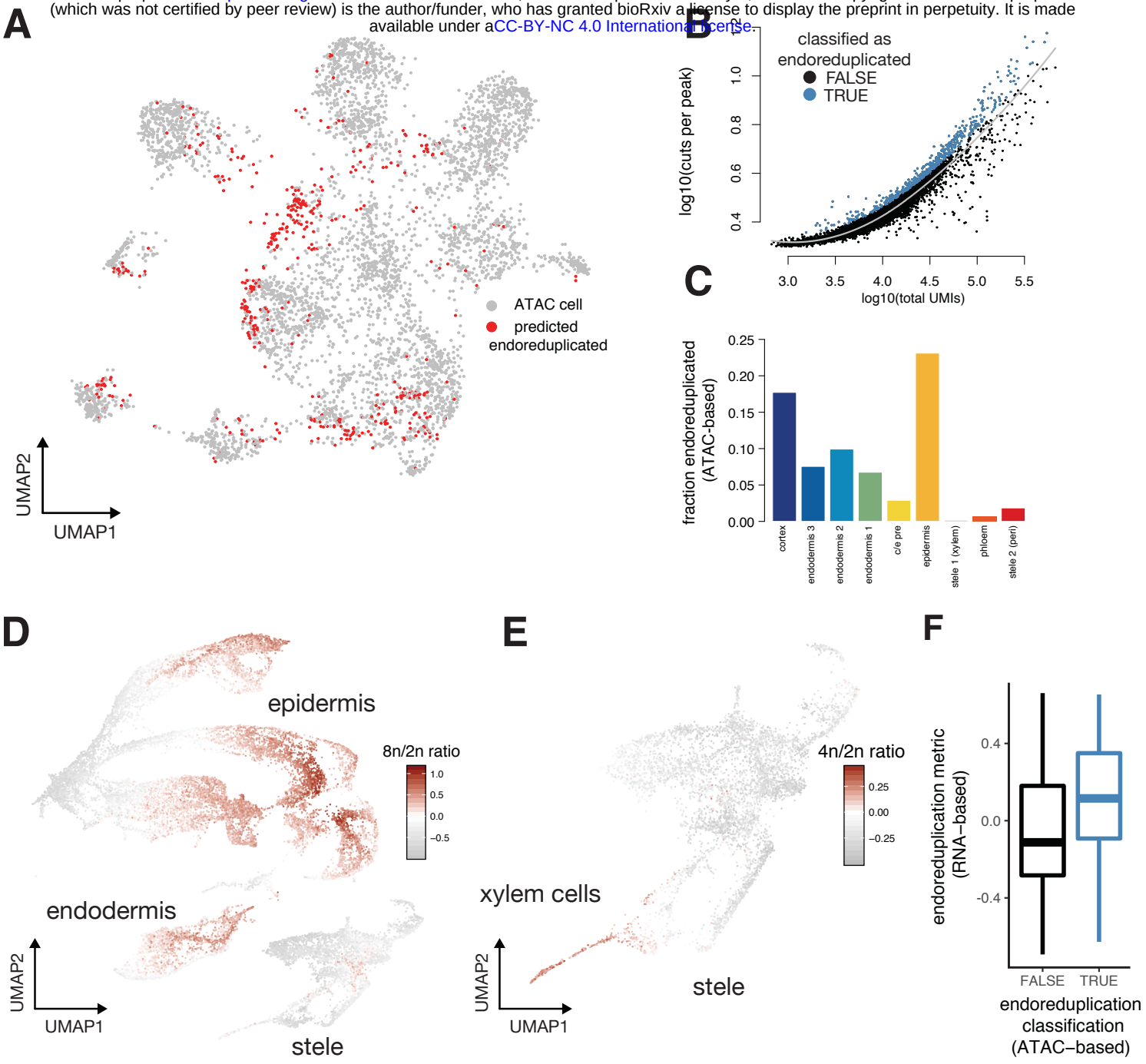

Supplementary Figure 4. Approaches for identifying endoreduplicated cells in both scATAC and scRNA-seq data.

Supplementary Figure 4. Approaches for identifying endoreduplicated cells in both scATAC and scRNA-seq data. (A) UMAP plot of root scATAC cells, each colored based on whether that cell surpasses a threshold level of cuts per site. Red denotes cells predicted as having undergone endoreduplication. (B) Scatterplot showing the relationship between total UMIs per cell (x-axis) and cuts per peak (y-axis); this relationship was captured in a Loess fit (black line), which was used to determine a threshold for cells with higher cuts per peak than expected based on their total UMIs (cells colored in blue, see Methods for more detail). (C) Barplot showing the fraction of cells in each type that showed putative endoreduplication, as determined by the threshold drawn in (B). In general, outer cell layers showed higher fractions of endoreduplicated cells, while cell layers of the stele showed lower levels. (D) UMAP of root scRNA cells, each colored based on the expression level of a transcriptional signature for endoreduplication, as determined by a ratio of expression levels in genes previously determined as enriched in 8n cells over those enriched in 2n cells.[19] (E) A known instance of endoreduplication in the stele, tetraploid xylem[19], is identified by a metric similar to (D), except that cells are colored by signature for 4n cells (ratio of 4n-specific genes to 2n-specific genes). (F) Boxplot showing the transcriptional-signature-based endoreduplication metric compared to a binary classification of endoreduplication cells using scATAC data. scATAC cells with high levels of cutcounts at a single locus (suggesting endoreduplication, as in A-C) were analyzed in the co-embedded graph with scRNA-seq cells to calculate the average level of the endoreduplication signature among each scATAC cell's 25 nearest neighbors. The overall trend shows that the cutcount-based classification of endoreduplication is consistent with the transcriptional-signature-based metric (one-sided student's t-test $p < 1E^{-14}$).

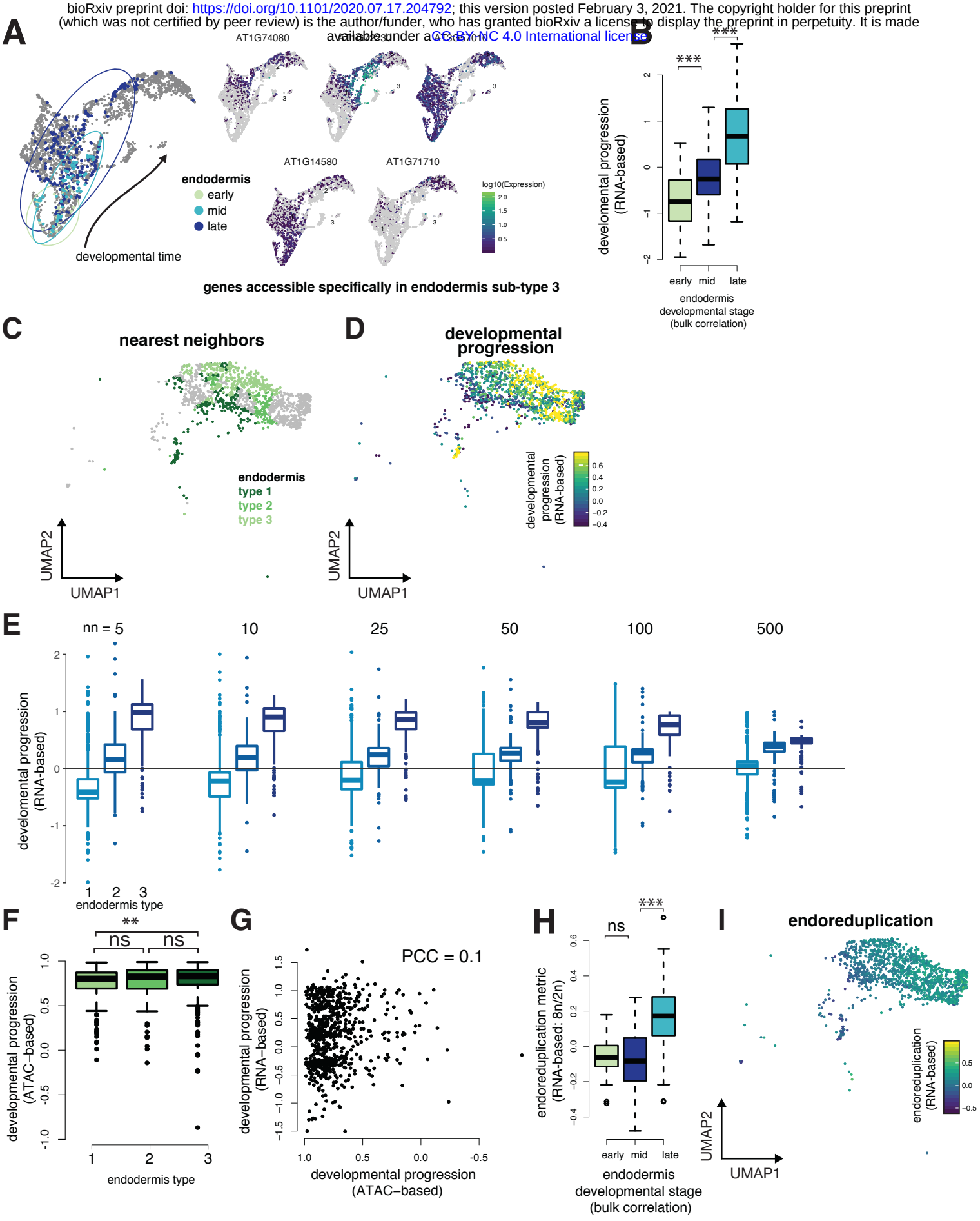

Supplementary Figure 5. Characterization of endodermal sub-types with combined scATAC and scRNA-seq data.

Supplementary Figure 5. Characterization of endodermal sub-types with combined scATAC and scRNA-seq data. (A) UMAP of endodermal cells from multiple scRNA-seq studies, with previously-determined developmental stages highlighted.[2] Inset shows variable expression patterns of genes with accessibility patterns specific to endodermal sub-type 3 in the scATAC data. (B) Boxplot showing that developmental progression scores are consistent with previously described annotations of developmental progression (early, middle, late) of the endodermis (all comparisons significant in one-sided students t-test $p < 1E^{-14}$).[2] (C) Subset of co-embedded UMAP from Figure 2A showing only endodermal cells; 25 nearest RNA neighbors for each endodermal type are indicated in shades of green. (D) As in (C), but shows RNA neighbor cells colored by transcription-based developmental progression metric. (E) Boxplots showing data from Figure 3C, with average developmental progression computed with different numbers of nearest neighbors. Above each plot, the number of neighboring cells (nn) from the scRNA-seq data used to predict developmental progression of each scATAC endodermal cell is shown. The relative differences in predicted developmental progression is insensitive to the number of nearest neighbors used in the procedure. (F) Boxplots showing levels of accessible genes (analogous to transcriptional complexity metric from Fig. 3C, only computed as total number of accessible genes rather than total number of transcribed genes). The overall trend remained the same, with progressive loss of complexity in the later endodermal types (significant for sub-type 1 vs 3, one-sided student's t-test p-value = 0.0032, not significant for other comparisons), but the ATAC-based metric showed less sensitivity than the RNA-based one. (G) Scatterplot showing poor correlation (PCC = Pearson correlation coefficient) of ATAC-based developmental progression score and the RNA-based score. (H) Boxplot as in (B), showing transcription-based endoreduplication scores (y-axis) for cells annotated for endodermal developmental stages by a previous scRNA-seq experiment (early and middle comparison not significant [ns], middle and late comparison, one-sided students t-test $p < 1E^{-14}$). (I) As in (D), with RNA neighbor cells colored by transcription-based endoreduplication metric.

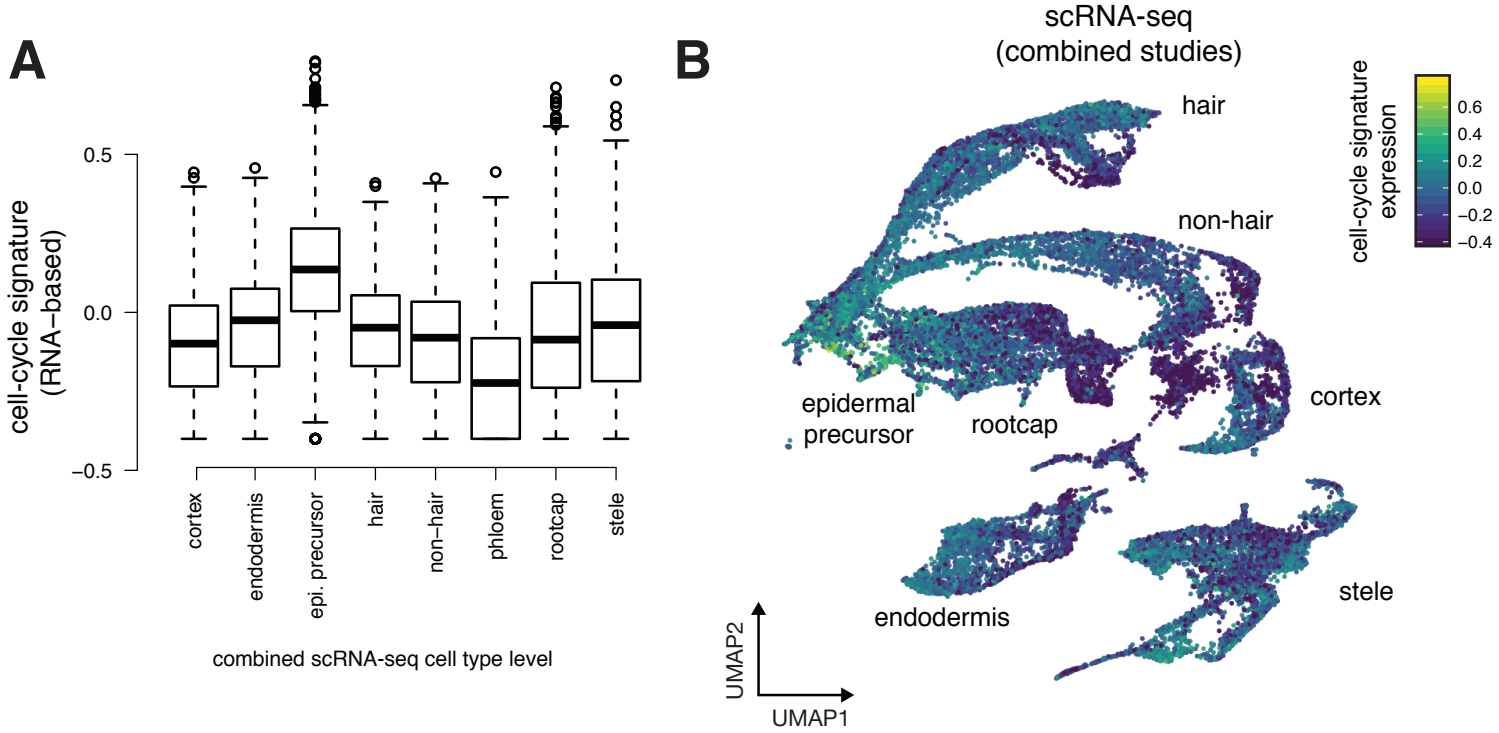

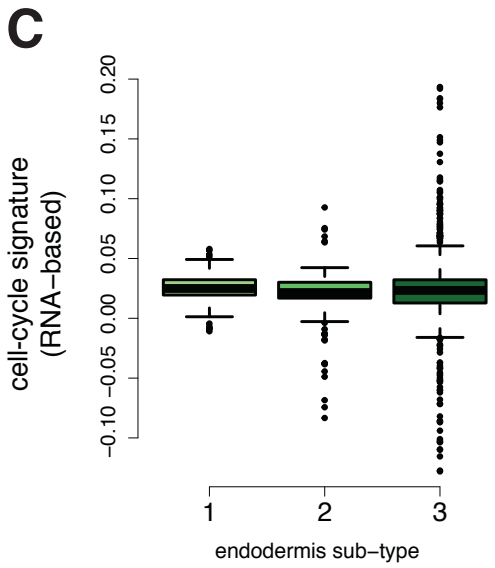

Supplementary Figure 6. Dividing cells are present in the root, but do not distinguish endodermis sub-types

Supplementary Figure 6. Dividing cells are present in the root, but do not distinguish endodermis types. (A) Boxplots showing levels of a cell-cycle signature in each scRNA-seq root cell type. (B) UMAP plot of combined root scRNA-seq studies with each cell colored by its expression the cell-cycle signature.[32] (C) Cell-cycle signature predicted from nearest neighbors of endodermis types (as in **Figure 3C, 3D**) shows that proliferation is not a strongly distinguishing feature between the sub-types.

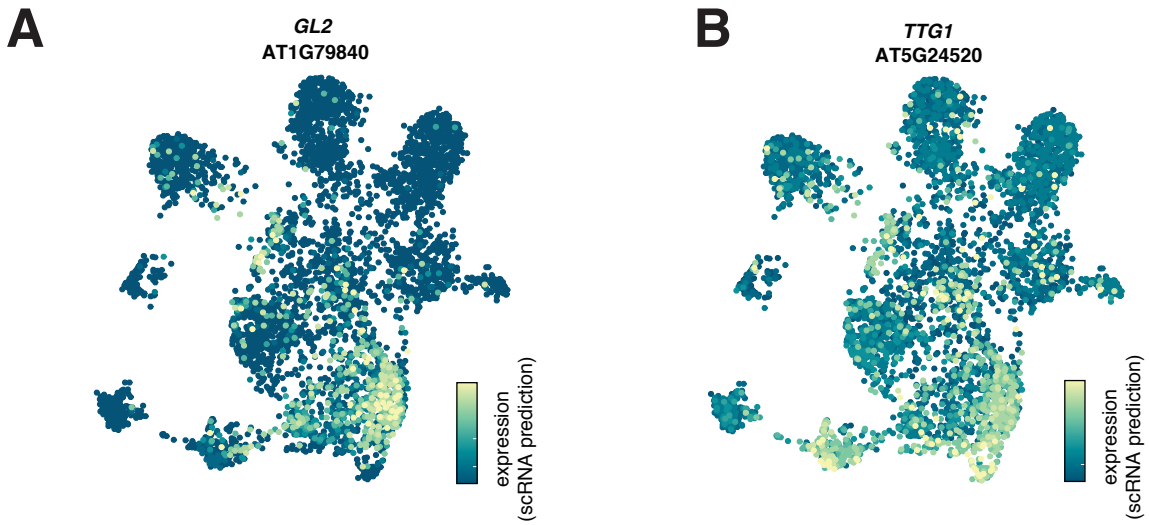

Supplementary Figure 7. Identifying transcription factors involved in tissue specification.

Supplementary Figure 7. Identifying transcription factors involved in tissue specification. (A) UMAP of scATAC cells colored by predicted expression level of epidermal specification factor *GL2.* (B) UMAP of scATAC cells colored by predicted expression level of epidermal specification factor *TTG1*.